IJE TRANSACTIONS B: Applications Vol. 34, No. 05, (May 2021) 1213-1224

International Journal of Engineering

Journal Homepage: www.ije.ir

Analytical Evaluation of Core Losses, Thermal Modelling and Insulation Lifespan Prediction for Induction Motor in Presence of Harmonic and Voltage Unbalance

M. Ghods[a], J. Faiz*[a], A. A. Pourmoosa[a], S. Khosrogorji[b]

[a] *Centre of Excellence on Applied Electromagnetic Systems, School of Electrical and Computer Engineering, College of Engineering, University of Tehran, Tehran, Iran*
[b] *Faculty of Electrical Engineering, University of Shahid Beheshti, Tehran, Iran*

PAPER INFO

Paper history:
Received 03 August 2020
Received in revised form 31 March 2021
Accepted 01 April 2021

Keywords:
Induction Motor
Thermal Modeling
Insulation Lifespan
Harmonic
Voltage Unbalance

ABSTRACT

Electrical motors are the ubiquitous workhorses of the industry, working over wide range of conditions and applications. Modern motors, designed to exact ratings using new materials and improved manufacturing techniques, are now much smaller but have higher loadings. They are being operated much close to the overload point than ever before. To ensure a satisfactory life span for the motor, temperature rise must be limited to the safe values. This paper proposes an analytical approach to estimate core losses of induction motor supplied by either harmonic content or voltage unbalance source. A thermal model based on the thermal lumped parameters is introduced and used to predict the insulation lifespan of the motors. Lumped parameters network of the motor is developed based on dimensions of the motor, thermal resistances, thermal capacitances, and loss sources. Then, the model is used to estimate the temperatures in different parts of the machine and the insulation lifespan of the motor. Finally, the predicted results using the model are verified by experiments.

doi: *10.5829/ije.2021.34.05b.14*

NOMENCLATURE

P_c	Core losses (W)	VUF	Voltage unbalance factor
k_h	Steinmetz coefficient	T	Maximum temprature (C)
f	Fundamental frequence (Hz)	F	Loading coefficient
P_e	Eddy current loss (W)	L_x	Percent lifespan at x%
B	Flux density (T)	HIC	Halving interval
k_e	Eddy current coefficient	T_c	Total permissible temperature of the insulation,
θ_h	Phase angle of the h^{th} harmonic	T_x	Hotspot temperature of the insulation

1. INTRODUCTION

Nowadays, inverter-fed drives are widely used in industries. The inverter output voltage contains some harmonics, and when variable speed drive (VSD) is supplied by this voltage the core losses of the machine increase. This affects both the efficiency and insulation lifespan of the motor. Besides, estimation of the core losses of the inverter-fed motor is more complicated than that of direct-supply motor [1-2].

Generally, core losses depend on the magnetic flux density and the supply frequency. The distorted input voltage of the motor leads to a non-sinusoidal flux density which increases the core losses. Therefore, accurate estimation of core losses at various conditions is essential in the optimal design of the motor. Owing to the non-uniform flux density in the machines, core loss analysis is a challenging problem. The core losses mainly consist of static and dynamic components. The static component is the hysteresis loss occurring even at zero frequency. The dynamic component is divided into eddy current losses and excess losses which is the result of magnetic domain walls variations. Since the components of the losses have different origins, they

* Corresponding Author Institutional Email: jfaiz@ut.ac.ir (J. Faiz)

Please cite this article as: M. Ghods, J. Faiz, A. A. Pourmoosa, S. Khosrogorji, Analytical Evaluation of Core Losses, Thermal Modelling and Insulation Lifespan Prediction for Induction Motor in Presence of Harmonic and Voltage Unbalance, International Journal of Engineering, Transactions B: Applications Vol. 34, No. 05, (2021) 1213-1224

must be decomposed into hysteresis losses, eddy current losses, and excess losses. The required parameters for core losses modelling are generally obtained from the experiments on the motors [3-6].

If the core losses in the inverter-fed motor are evaluated considering only the fundamental harmonic of the flux density, the estimated losses are certainly underestimated [7-8]. The flux density differs in various parts of the motor, and the core losses are not identical in different parts of the machine [9]. The most precise method for estimating the core losses is the finite element method (FEM) [10-17]. However, precise prediction of the flux density in the actual motor is a difficult task. The method demonstrated by Bradley et al. [10] can estimate the core losses generated by the distorted voltage. The stator core losses have been calculated for a no-load motor by Gyselinck et al. [11], while the rotor core losses have been ignored due to the low-frequency current in the rotor. Also, a method introduced by Boglietti et al. [14] can evaluate the core losses in the different parts of the stator of an inverter-fed induction motor. The impact of the core losses on induction motor parameters has been discussed by [16]. The classical model of calculating the core losses has been presented in literature [18-19]. When the frequency or the flux density is relatively low, the accuracy of the classical model is reasonable. A fast core loss on induction motor has been estimated based on the piecewise variable parameter model by Zhao et al. [20] which considers the voltage harmonic components of the inverter. The rotational losses have been reported by Alatawneh N., and Pillay, [21] in which the effect of minor loops on the core losses have been taken into account. Moreover, an improved generalized Steinmetz equation has been proposed by Venkatachalam et al. [22].

The core losses might cause an overheating in different parts of an electrical machine and decline its performance. Therefore, thermal analysis of the machine plays an important role in the design stage of electrical machines. This analysis can help the designers to design a minimum size and weight machine for certain torque or power. Moreover, in applications where a high-performance motor is required, accurate thermal modelling is crucial [23]. Thermal modelling for stator winding in short-term transient has been proposed in literature [24-25]. Thermal analysis of induction motors has been addressed in literature [26-31]. The thermal behaviour of induction motors in a wash-down environment has been discussed by Jankowski et al. [26], in which thermal properties of the motors have been considered. Different classes of induction motors, in terms of protection requirements, have been discussed by Fernando et al. [28]. The end-winding thermal effect of induction motor has been analyzed by Ahmed and Kar [29] in which the predicted stator winding temperature using a 1st-order and higher-order thermal model has been compared. The thermal model lumped parameters of wound-rotor induction motor and their analytical equations have been given by Boglietti et al. [30].

The first contribution of the present paper is to introduce a core losses estimation method that can calculate losses in the presence of harmonics and voltage unbalance. Compared to the available models, the proposed model has two important features. Firstly, eddy current and hysteresis coefficients are directly expressed as a function of the flux density and then these flux density-dependent coefficients are estimated using the curve fitting technique, while in the existing methods two steps are required to calculate the coefficients. Secondly, unlike available methods, excess losses in the proposed method is not initially considered in the losses equation, but after applying curve fitting and finding coefficients for eddy current and hysteresis losses, the remaining coefficient is the coefficient of excess losses. The second contribution of this paper is to propose a thermal analysis for induction motor when it is supplied by a distorted voltage or exposed to a voltage unbalance. The proposed modelling is a combination of FEA and analytical techniques. The rest of the paper is organized as follows: Section 2 proposes an analytical method based on the curve fitting technique through which the core losses in electrical machines are estimated, and its accuracy is discussed in section 3, then the estimated results are compared to those obtained experimentally. Section 4 presents the thermal model of induction motor in the presence of harmonics and voltage unbalance. The accuracy of the proposed thermal modelling is validated by the test results in section 5. In section 6, the insulation lifespan of the motor is discussed and the lifespan of the motor in the presence of harmonics and voltage unbalance is predicted. Section 7 concludes the paper.

2. CORE LOSSES ESTIMATION METHOD

The core losses influence the performance and shorten the lifespan of the inverter-fed induction motors. Therefore, it is crucial to precisely estimate the core losses caused by the various harmonic components of the magnetic fluxes. At this end, the waveforms of flux densities in different parts of the machine structure must be known. The non-sinusoidal waveforms of flux densities, depending on the amplitude and harmonic order, may generate some minor loops in the magnetization characteristic. For the magnetic flux density less than 1 T with fundamental frequency, the core losses are divided into hysteresis losses (P_h) and eddy current losses (P_e) as follows:

$$P_c=P_h+P_e=k_h f B_m^n+k_e f^2 B_m^2 \quad (1)$$

A curve fitting technique is applied in which the core losses are divided into eddy current losses and hysteresis losses. However, compared to the existing models for core losses estimation, the proposed model has two

important features. Firstly, eddy current and hysteresis coefficients in the model are directly expressed as a function of the flux density and then these coefficients are estimated using the curve fitting technique, while in the existing methods, two steps are required to estimate the hysteresis coefficient k_h. The Steinmetz coefficient and k_h are separately estimated using the curve fitting technique. Secondly, to include the excess losses in the existing method, a new coefficient is proposed and determined using the curve fitting technique; however, it was not initially considered in the losses formula previously, but it is taken into account after curve fitting and finding coefficients for eddy current and hysteresis losses. Based on the above-discussed items, the steps for estimating the core losses are given as follows:
Step I: defining the total core losses as follows:

$$P_c=k_h(\mathrm{f,B})\,f+k_e(\mathrm{f,B})\,f^2 \tag{2}$$

Step II: dividing the total core losses by square root of frequency as follows:

$$\frac{P_c}{\sqrt{f}}=k_h(\mathrm{f,B})\sqrt{f}+k_e(\mathrm{f,B})\,f\sqrt{f} \tag{3}$$

Step III: for different values of flux density, $P_c/\sqrt{f}$ versus square root of frequency is plotted and then a cubic spline fitting technique is applied to each value of the flux density as follows [36]:

$$\frac{P_c}{\sqrt{f}}=a_3\sqrt{f}^3+a_2\sqrt{f}^2+a_1\sqrt{f}+a_0 \tag{4}$$

Step IV: by comparing Equation (3) with Equation (4), a_1 is k_h(f,B) and a_3 is k_e(f,B). Also, this comparison shows that the right-hand side of Equation (2) must include an additional term. This additional term is called excess losses. Therefore, the total core losses are rewritten as follows [36]:

$$P_c=k_h(\mathrm{f,B})\,f+k_e(\mathrm{f,B})\,f^2+k_{ex1}(\mathrm{f,B})\,f^{1.5}+k_{ex2}(\mathrm{f,B})\,f^{0.5} \tag{5}$$

where k_{ex1}(f, B) and k_{ex2}(f, B) are the excess losses coefficients.

The cubic spline fitting of the specific core losses and finding the coefficients in terms of the flux density enables us to estimate these coefficients at any flux density. Using the proposed model, one can easily estimate the total core losses for any flux density which in turn prevents underestimation of the core losses at high-frequency harmonics and its overestimation at low-frequency harmonics.

2. 1. Core Losses in Presence of Harmonics

Core losses under alternating pulse voltage excitation have been predicted in literature [34-36]. In the method, three components of core losses, as well as the form factor of the harmonic voltage, have been used to estimate the losses. Suppose distorted input voltage of the motor is as follows:

$$V(\mathrm{t})=\sum_{h=1,2,\ldots} V_h\cos(\mathrm{h}\,2\pi\,ft+\theta_h) \tag{6}$$

where h is the harmonic order, V_h is the amplitude of the h^{th} harmonic of the phase voltage, and θ_h is the phase angle of the h^{th} harmonic. The magnetic flux density in the core generated by the applied voltage is as follows:

$$B(\mathrm{t})=\sum_{h=1,2,\ldots} B_h\sin(\mathrm{h}\,2\pi\,ft+\theta_h) \tag{7}$$

where B_h is the amplitude of the h^{th} harmonic of the flux density. Therefore, in the presence of harmonics, the peak flux density is as follows:

$$B=\sqrt{\sum_{h=1,2,\ldots} h^2B_h^2} \tag{8}$$

When a distorted voltage is applied to the motor, the hysteresis, eddy current and excess losses coefficients corresponding to the flux density shown in Equation (1) should be determined for estimation of the core losses.

2. 2. Core Losses in Presence of Voltage Unbalance

Unbalanced voltage may apply to the induction motor. The IEEE standard gives the following definition for VUF:

$$VUF=\frac{V^-}{V^+}\times 100\% \tag{9}$$

where V^+ and V^- are the positive and negative sequence voltage components, respectively. Since V^+ and V^- are phasors, the *VUF* has magnitude and angle. These components can be calculated using the fast Fourier transform or Fortescue transform. Similar to the method used to estimate the core losses in the presence of distorted voltage, the hysteresis, eddy current and excess losses coefficients, corresponding to the flux density generated by the voltage unbalance, can be derived from Equation (5) and used for the core losses estimation.

2. 3. Different Methods of Core Losses Estimation

2. 3. 1. Epstein Frame Epstein frame is the most popular method for experimental core losses estimation. The IEC 404-2 describes the structure of the Epstein frame in detail. The standard structure for the Epstein frame is a 28 cm×28 cm frame with four coils of 700 turns on the primary and the secondary. The primary winding or magnetizing winding is wound onto the secondary winding or voltage winding. The samples are located on the frame, so that a double-lapped joint is created. By multiplying the primary winding current and the secondary winding voltage, the instantaneous power loss is obtained. Then, the total core losses are determined by averaging the instantaneous power. To

find the specific total losses, the total losses are divided by the weight of the sample. The main disadvantage of the Epstein frame is the generated leakage flux around the joint leading to the non-uniform flux density distribution. Besides, the impact of the harmonic components on the total core losses cannot be evaluated using the standard frame.

2. 3. 2. Toroid Tester The structure of the toroid tester is very similar to that of the Epstein frame. The only difference is that the specimen in the toroid tester is a wound toroid. For small electrical motors, the total losses obtained from the toroid tester is more accurate than those achieved by the Epstein frame. Like the Epstein frame, non-uniform flux density distribution is one of the problems with the toroid tester. Moreover, the toroid tester method is more time-consuming than the Epstein frame method. The reason is that the toroidal winding must be appropriately wound onto the core. It is noted that the toroid tester configuration is much more similar to the structure of a stator in conventional electric motors, making it preferable for calculating the core losses over the Epstein frame method.

2. 3. 3. Single Sheet Tester Compared to the existing methods, the single sheet tester is a simple and economic way for measuring the core losses. In this method, an excitation coil with a low number of turns is wound around a double-yoke sheet. The flux generated by the coil in the yoke produces a current which in turn generates power losses in the sheet. The single sheet tester has two disadvantages. First, the double yoke is large and costly. Second, the tester needs to be calibrated with either the toroid tester or the Epstein frame.

3. TEST SETUP FOR CORE LOSSES MEASUREMENT

To validate the proposed method for core losses estimation, the obtained results by applying the method are compared with the measured core losses. To produce a desired magnetic flux density in the core, a toroid tester, as well as a signal generator, are used. The signal is generated by a single-phase inverter, supplying the toroid transformer. The magnetic flux is produced by the applied signal and induced voltage in the secondary winding. Therefore, the measured current in the primary and measured voltage in the secondary winding corresponds to the magnetic flux intensity and the flux density, respectively. Flux density is obtained by integrating the secondary voltage. Besides, a filter is employed in the output of the inverter to reduce the voltage pulsation. Figure 1 demonstrates the test setup.

Figure 2 compares the predicted core losses using the proposed method and the experimental results. A good agreement between the predicted and test results is

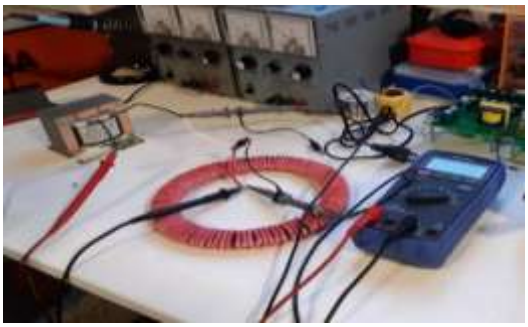

Figure 1. Toroid tester setup

achieved. Figure 3 demonstrates the minor loop on the magnetization characteristic for the distorted magnetic flux density. The minor loop in Figure 3 has been created by 10% of 5th harmonic.

4. THERMAL MODELLING OF INDUCTION MOTOR IN PRENSENCE OF HARMONIC AND VOLTAGE UNBALANCE

The main heat-generating sources in electrical machines are electrical, magnetic, and mechanical losses. In a variable speed drive, the produced harmonics by the inverter lead to more losses compared with the motor directly supplied by mains. It is noted that the impact of harmonics on the core loses is more prominent. As a result, in the presence of harmonics, temperature rise in different parts of the motor are more pronounced. A similar problem is true when the motor is supplied by voltage unbalance. Therefore, thermal modeling of electrical machines in the presence of the harmonics and voltage unbalance are necessary in its design stage. In this section, the main objective is to provide a thermal analysis for an induction motor supplied by a distorted voltage or voltage unbalance. The proposed modeling is a combination of FEA and analytical techniques.

Taking into account all the above-mentioned items, the thermal modeming steps of the induction motor are as follows:

1st Step: To determine the flux density at different parts of the motor, harmonic voltage is applied to the stator winding which is simulated by the Ansoft.

2nd *Step*: Using Equation (1) and the magnetic flux density obtained from the 1st step, the core losses in different parts of the motor such as stator yoke, rotor yoke, and stator teeth, are estimated. The core losses for each part are then divided by its weight through which specific core losses are estimated. Besides, the copper losses.

3rd Step: Using the motor data such as dimensions and number of stator slots, lumped thermal network of the motor is implemented in the Motor-CAD software, which is a tool for the thermal analysis of electrical

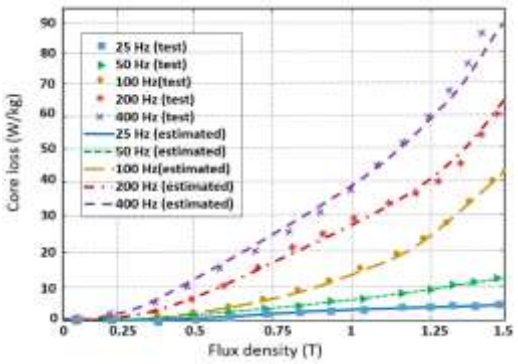

Figure 2. Core losses curve cluster of various frequencies at 50 °C

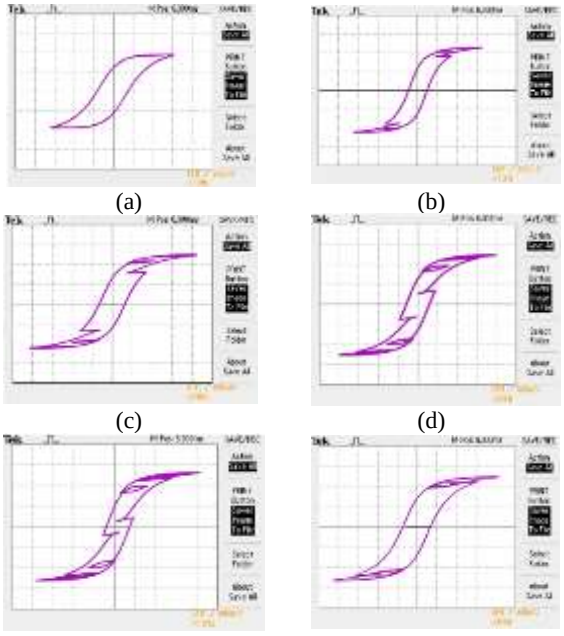

Figure 3. Magnetization characteristics. (a) 1st component, (b) 1st and 10% - 5th harmonic, (c) 1st and 10% - 7th harmonic ,(d) 1st and 10% - 11th harmonic (e) 1st and 10% - 13th harmonic, (f) 1st and 5th , 7th, 11th, 13th harmonics are obtained by simulation.

machines. By solving the lumped thermal circuit, the temperature in various parts of the motor are determined. *4th Step:* Using the results obtained from in the 3rd step, the insulation lifespan of the motor is estimated. Figure 4 depicts the flowchart of the thermal analysis of the induction motor.

4. 1. FEM Analysis of Proposed Motor Table 1 summarizes the specifications of the proposed induction motor. Figure 5 shows the 3D view of the motor. Figure 6 illustrates the magnetic flux density distribution in different parts of the motor when a distorted voltage is applied to the stator winding. In each case, the voltage is

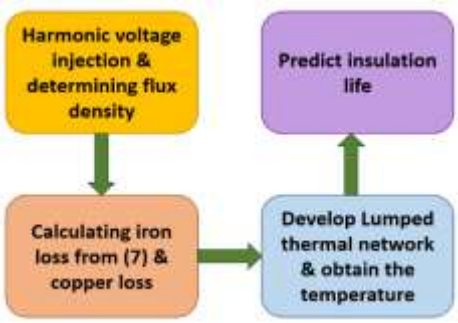

Figure 4. Flowchart for thermal analysis of induction motor

TABLE 1. Motor Specifications

Parameter	Value
Line voltage (V)	380
Frequency (Hz)	50
Number of poles	4
Rated current (A)	2
Rated torque (Nm)	5
Output power (W)	750
Efficiency (%)	79
Power factor	0.707

Figure 5. 3D view of proposed motor

the sum of the fundamental component of the voltage and the percentage of a certain high-order harmonic. For example, in Figure 6a, the fundamental component with 10% of the 5th harmonic is applied to the stator winding. It is observed that the impact of the unbalanced voltage on the magnetic flux density is more than that of the distorted voltage. Figure 7 shows the core and copper losses variations for different harmonic. As seen, voltage unbalance causes the increase of both copper and core losses compared to the balanced voltage. Also, the lower the harmonic order, the higher the losses.

4. 2. Thermal Modelling In this section, the impact of the distorted voltage as well as voltage unbalances on the temperature rise of various parts of the induction motor are predicted using the proposed thermal modeming. Motor-CAD software is used to model the thermal behaviour of the motor as shown in Figure 8. To

implement the model, general data such as dimensions, number of stator and rotor slots (39/20), and number of rotor bars are needed. The data then is used to develop the thermal model of the motor. The model consists of a set of thermal resistors, thermal capacitors, and thermal

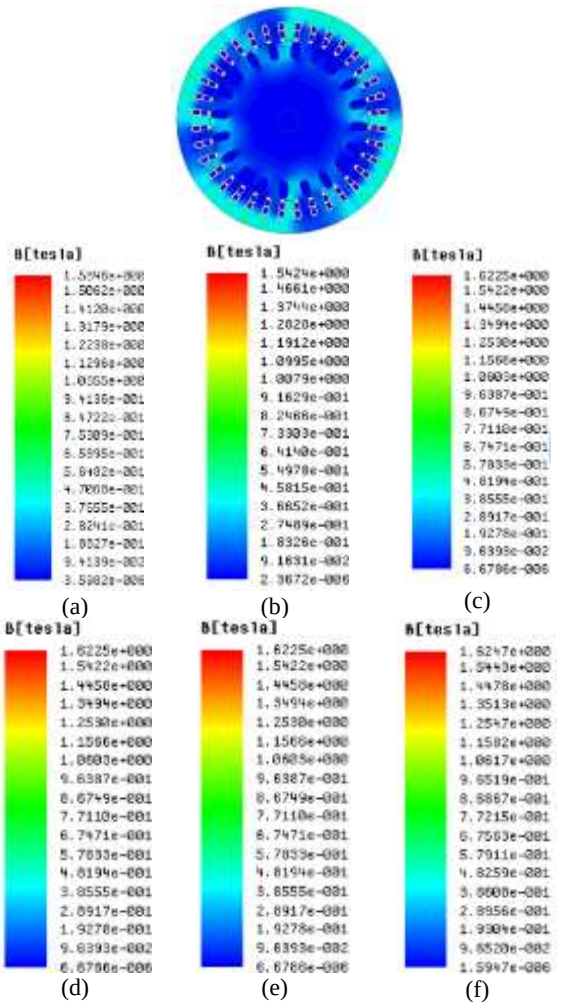

Figure 6. Flux density distribution. (a) 1st component, (b) 1st and 10% of 5th harmonic, (c) 1st and 10% of 7th harmonic,(d) 1st and 10% of 11th harmonic (e) 1st and 10% of 13th harmonic, (f) 1st and 5th , 7th, 11th, 13th harmonics

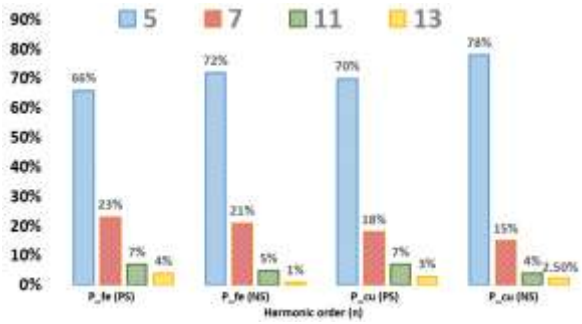

Figure 7. Iron and copper loss variations for different harmonic (PS: Positive seq. and NS: Negative seq.)

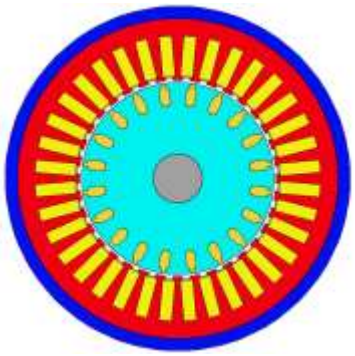

Figure 8. proposed motor in Motor-CAD

sources. Figure 9a depicts the lumped parameter network (LPN) of the motor. Since the objective is to analyse the motor at steady-state, the thermal capacitors are not considered in the model. The values of the thermal sources are obtained from the losses calculated in the 3rd step. It is noted that the nodes in the LPN demonstrate the temperature at different parts of the motor. Figure 9b presents the thermal resistors and thermal sources corresponding to the LPN (Figure 9a).

The thermal equivalent circuit (TEC) shown in Figure 9b consists of 49 thermal resistors and 15 thermal sources. The definition of each resistor as well as the definition and value of each thermal source have been summarized in Tables 2 and 3, respectively. According to Table 3, the thermal source for each part of the motor corresponds to the estimated losses of that part. The estimated losses for each part are expressed in percentage of the total losses calculated in the presence of the harmonic or voltage unbalance. To obtain the temperature at each node, the network shown in Figure 9b is implemented in Power-sim software as shown in Figure 10. In this case, the TEC is treated as an equivalent electrical circuit and as a result, the temperature at each part of the motor is estimated. The stator and rotor copper losses for the proposed motor at different harmonic and unbalanced conditions are tabulated in Table 4.

5. EXPRIMENTAL SETUP

To validate the accuracy of the proposed thermal model, the induction motor was tested and the experimental results were compared to those obtained by the proposed method. Figures 11a and 11b show the stator and rotor of the motor. Figure 11c presents the experimental test setup. To generate harmonic-polluted voltage, ARM microcontroller was used to build the input voltage with different harmonic contents as well as voltage unbalance. The digital oscilloscope stored this voltage and the current sensor (LTS25) measured the current. Also, to measure the winding temperature a sensor (PT100) was located in the stator winding. Moreover, a thermo-couple measured the temperature in different parts of the motor.

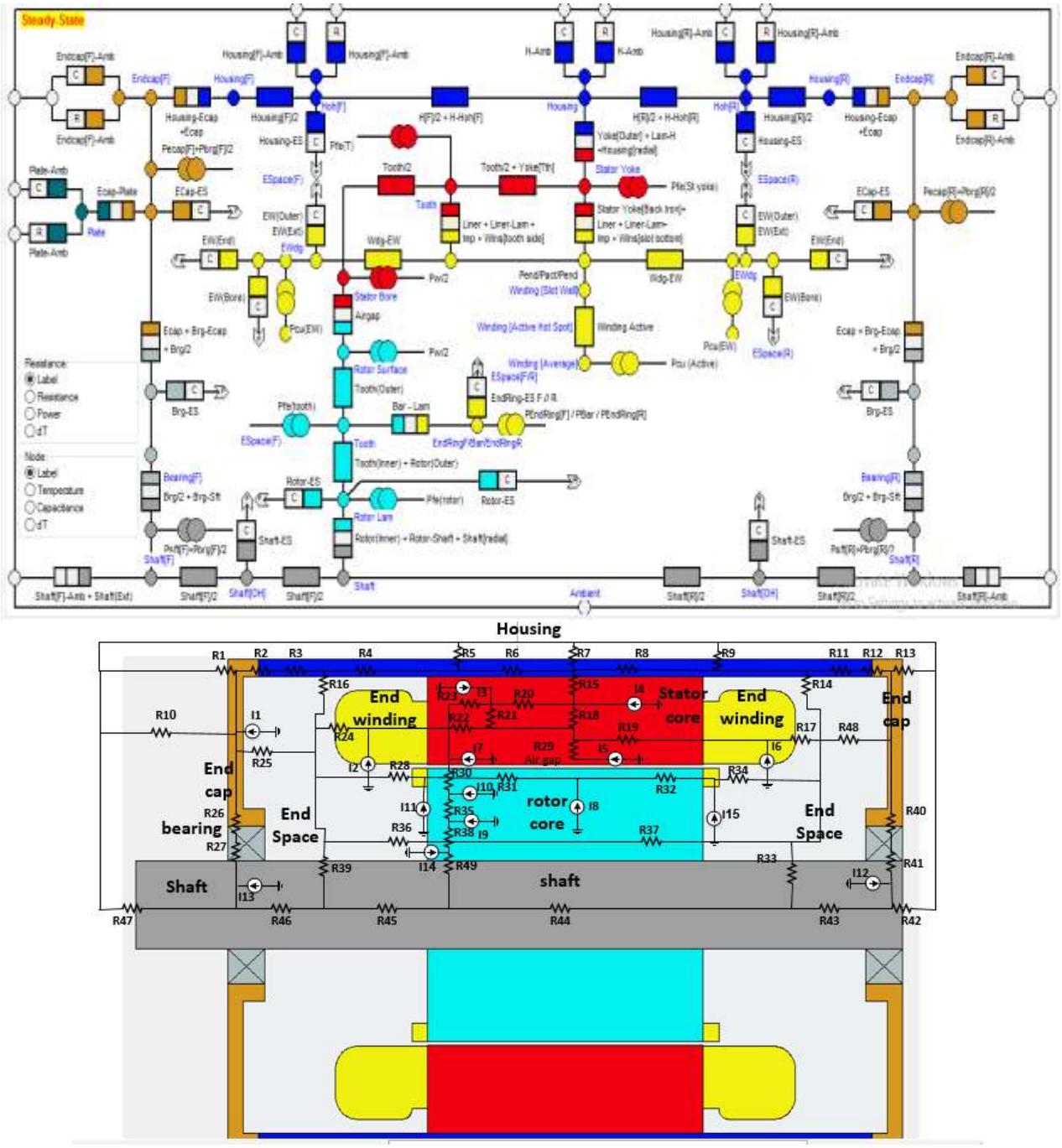

Figure 9. Lumped parameters model: (upper) lumped network, (lower) thermal equivalent circuit

TABLE 2. Thermal model resistances

Convective resistance of cap to environment (R_1 , R_{13})
Conductive resistance of the body (R_3,R_4,R_6,R_8,R_{11})
Resistance between cap and plate to environment (R_{10})
Conductive resistance between body and stator yoke (R_{15})
Convective resistance between stator end-winding and indoor air (R_{24} , R_{17})
Yoke and stator teeth convective resistance (R_{20})
Convective resistance between indoor air and cap (R_{25} , R_{48})
Conductive resistance between bearing and shaft (R_{27} , R_{41})
Winding and rotor conductive resistance (R_{29}), (R_{31}, R_{32})
Shaft conductive resistance (R_{43},R_{44},R_{45},R_{46})
Conductive resistance between body and cap (R12 ,R2)

Convective resistance of body to air (R_5,R_7,R_9)
Convective resistance between a body with indoor air (R_{14},R_{16})
Convective resistance between yoke and stator winding (R_{18},R_{21})
Conductive resistance between stator end-winding and winding (R_{19},R_{22})
Conductive resistance teeth stator (R_{23})
Conductive resistance between cap and bearing (R_{26}, R_{40})
Conductive resistance between rotor load and indoor air (R_{28}, R_{34})
Convective resistance between rotor and stator core (R_{30})
Convective resistance between shaft and indoor air (R_{33},R_{39},R_{47},R_{42})
Convective resistance between rotor core and shaft (R_{49})

TABLE 3. Heat sources values

Heat source	Value (% Total loss)
Cap loss (I_1)	1
Stator end-winding loss (I_2,I_6)	11
Stator tooth loss (I_3)	20
Stator yoke loss (I_4)	15
Stator winding loss (I_5)	17
Stator bore loss (I_7)	1
Rotor bar loss (I_8)	12
Rotor core loss (I_9,$I_{10}$$I_{14}$)	16
Rotor shaft loss (I_{13},I_{12})	6
Rotor end-ring loss (I_{11},I_{15})	1

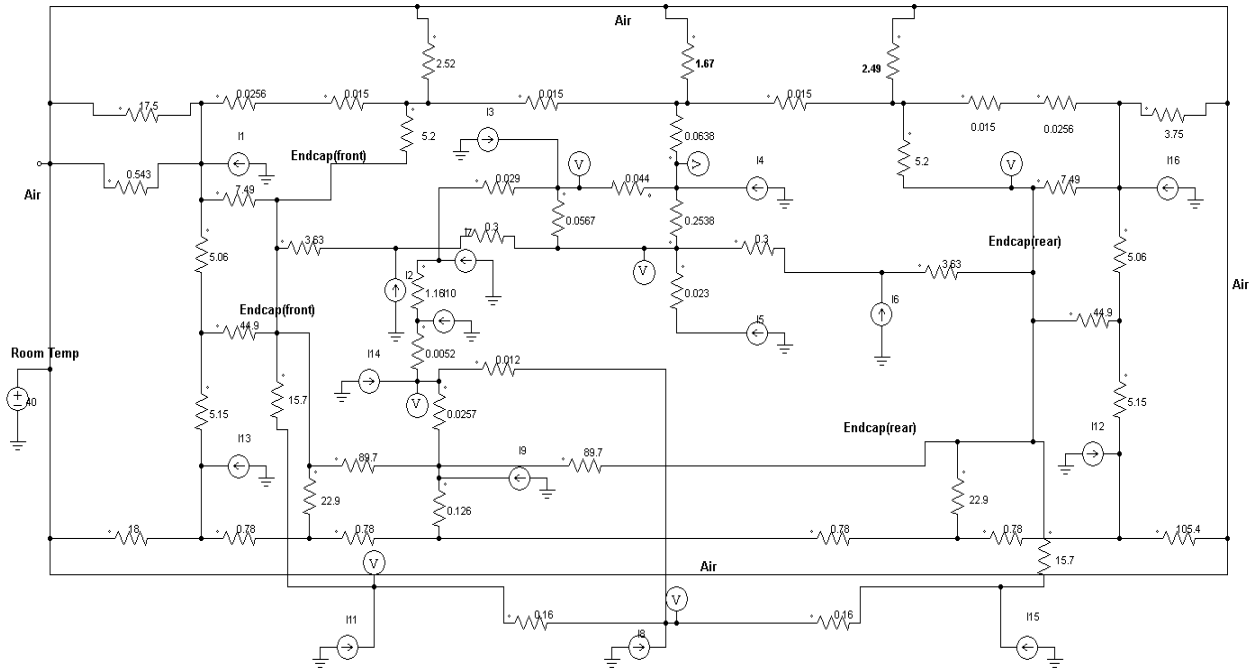

Figure 10. Lumped parameter model of proposed induction motor in Power-sim software

TABLE 4. Stator and rotor copper losses in harmonic and unbalanced voltage conditions

Harmonic Unbalance	Stator end winding loss (W)	Stator winding loss (W)	Rotor end-ring loss (W)	Rotor bar loss (W)
1st	22.4	33.7	12.5	24.9
5th	0.93	1.41	0.52	1.04
7th	1.11	0.74	0.68	1.36
11th	0.62	0.93	0.34	0.69
13th	0.5	0.75	0.29	0.58
5% unb	1.22	1.83	0.71	1.43
10% unb	1.70	2.55	0.99	1.98

6. RESULTS AND DISCUSSION

Table 5 summarizes the comparison between the measured temperature and the temperature obtained from the proposed thermal model at various parts of the motor for different harmonic contents and voltage unbalance. It is assumed that the ambient temperature is 40°C. The obtained results indicate that the high flux density leading to the high core losses generates the hotspot of the motor somewhere between the rotor conductors close to the stator. Besides, by rising the harmonic order, the temperature at different parts of the motor also increases. Moreover, Table 6 shows that the impact of the voltage unbalance on the temperature rise of the motor is more

than that of harmonic voltage. For example, the temperature rise of the rotor core is about 16% for 10% voltage unbalance. Also, when the voltage unbalance increases, the losses and as a result the temperature rise of the motor increase. Table 6 compares the measured core and copper losses and the losses obtained by the analytical method.

Figure 12 illustrates the input current waveform for different harmonic voltages applied to the stator winding. According to Figure 12, harmonic and unbalanced currents are generated by the drive and the output voltage of the drive (with harmonic and unbalanced) is applied to the stator winding. Then, with the help of P100 temperature sensors located in the accessible points inside of the motor, the temperature is measured and presented in Table 5.

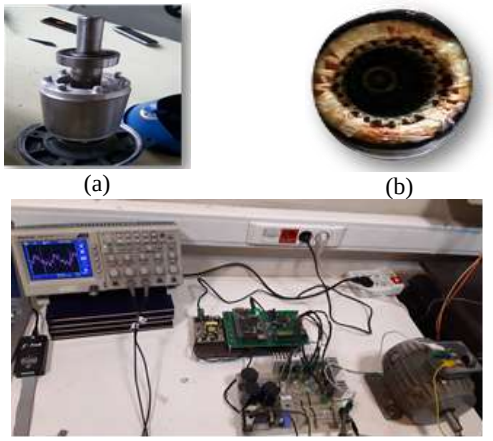

(a) (b) (c)

Figure 11. Experiment (a) stator, (b) rotor, and (c) test-bed

TABLE 5. Comparison of measured and simulated temperature at various parts of motor for different harmonic contents and voltage unbalance (Simulation - **Experimental**)

Unbalanced Harmonic	Stator yoke (°C)		Stator tooth (°C)		Stator end winding (°C)		Stator winding (°C)		Rotor Core (°C)		Rotor bar (°C)		Rotor end-ring (°C)	
1st	80.40	**83**	84.01	**86**	83.34	**86**	85.45	**87**	107.61	**112**	107.47	**112**	84.40	**88**
5th	82.65	**85**	89.25	**94**	89.61	**91**	89.76	**93**	111.01	**115**	111.15	**114**	92.70	**96**
7th	82.57	**86**	87.21	**90**	87.57	**88**	88.12	**91**	107.86	**114**	107.87	**109**	91.56	**94**
11th	81.51	**90**	87.11	**90**	86.48	**88**	87.78	**91**	107.77	**114**	107.62	**109**	91.47	**94**
13th	81.44	**92**	87.05	**91**	86.37	**89**	87.56	**90**	107.64	**117**	107.53	**109**	90.42	**94**
5% unb	94.84	**97**	95.44	**100**	95.81	**100**	96.14	**101**	108.41	**115**	108.26	**110**	98.89	**100**
10% unb	97.98	**101**	99.65	**103**	97.04	**104**	101.65	**107**	110.18	**117**	110.03	**114**	101.13	**106**

TABLE 6. Total losses in harmonic and voltage unbalance conditions

Harmonic Unbalance	Core losses (W) (sim.)	Core losses (W) (exp.)	Copper loss (W) (sim.)	Copper loss (W) (exp.)
1st	64.60	67.00	93.50	98.00
5th	4.4	4.6	3.9	4.12
7th	3.8	4.0	3.1	3.30
11th	3.1	3.3	2.6	2.70
13th	2.9	3.0	2.1	2.30
5% unb	5.0	5.1	5.1	5.70
10% unb	6.2	6.7	7.1	7.80

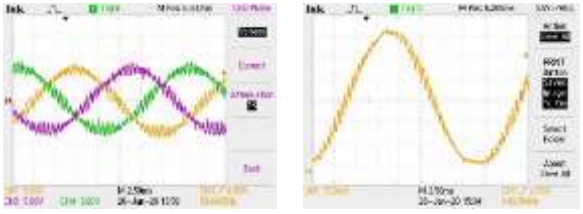

(a) (b)

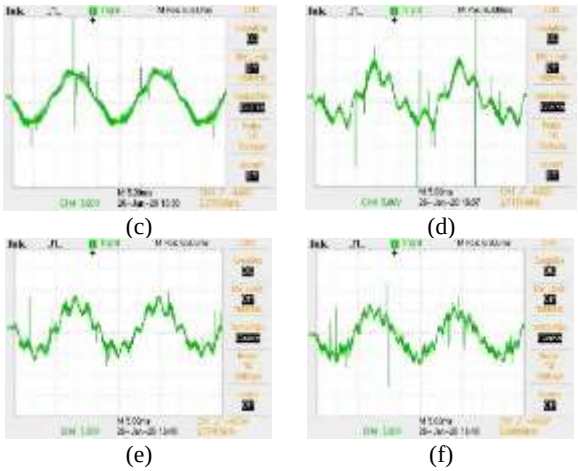

(c) (d) (e) (f)

Figure 12. Input current waveform. (a) three phase , (b) 1st component (c) 1st and 10% - 5th harmonic, (d) 1st and 10% - 7th harmonic ,(e) 1st and 10% - 11th harmonic (f) 1st and 10% - 13th harmonic

7. LIFESPAN ANALYSIS OF INDUCTION MOTOR INSULATION

After determining the temperature at different parts of the motor, the analysis shows that the maximum temperature

occurs in the rotor end ring because the magnetic flux density at the end ring is high compared to other parts of the motor. Since the insulation material is not used in the rotor of the squirrel-cage induction motor, the temperature rise of the end ring does not affect the insulation lifespan. Inspecting the temperature at different parts of the motor insulation, it is found that the stator winding experiences the maximum temperature. Therefore, the stator winding insulation reduces the lifespan of the motor. Assuming that the motor operates at 90% of the rated load, the maximum temperature of the motor insulation is as follows [35]:

$$T=F\times\Delta T+40 \quad (10)$$

where F is the loading coefficient of the motor (Table 7), and ΔT is the maximum temperature rise withstood by the motor in the desired insulation class. Since the proposed motor is a class A motor, from Equation (10), the maximum temperature of the motor insulation (T) is found to be 97.2°C. To obtain the insulation lifespan of the motor, the following equation can be used [35]:

$$L_x=L_{100\%}\times 2^{[\frac{T_c-T_x}{HIC}]} \quad (11)$$

where L_x is the percent lifespan at $x\%$ of rated load, L_{100} is the percent lifespan at rated load, T_c is the total permissible temperature of the insulation, T_x is the hotspot temperature of the insulation, and HIC is the halving interval. Using Equation (11), the insulation lifespan of the motor in the presence of harmonics and voltage unbalance are calculated and listed in Table 7.

The reason for the longer insulation lifespan at 90% of the rated load compared to the rated loading is the lower operating temperature compared to the maximum insulation temperature. Table 8 indicates that the effect of harmonic on the insulation temperature rise is low because of the low amplitude of the harmonic component compared to the fundamental one. This in turn leads to a small insulation temperature rise. However, even this small value dramatically affects the insulation lifespan of the motor. For example, 10% 5th harmonic results in the insulation temperature rise by 4.31°C, but it decreases the insulation lifespan of the motor by 376 days. The results also show that the impact of voltage unbalance on the decrease of insulation lifespan is more than that of harmonic voltage.

TABLE 7. F coefficients

Load (%)	F	Load (%)	F
50	52	110	119
75	73	115	130
90	88	125	146
100	100	150	212

TABLE 8. Lifespan prediction of the motor understudy at different harmonic and voltage unbalances (for 3000 days)

Harmonic Unbalanced	Maximum Temperature of insulation (C°)	Temperature variations at 90% of rated load (C°)	Lifespan variations at 90% of rated load (days)
1st	85.45	0	0
5th	89.76	4.31	-376
7th	88.12	2.67	-296
11th	87.78	2.33	-254
13th	87.56	2.11	-212
5% unb	96.14	13.69	-996
10% unb	101.65	16.20	-1114

8. CONCLUSION

This paper demonstrated an analytical method based on the curve fitting technique for calculating the core losses for induction motors. In this method, unlike the existing methods, the excess losses were not initially considered in the losses equation but after curve fitting and finding coefficients for eddy current and hysteresis losses, the excess losses coefficient was automatically extracted. Also, thermal modeling for insulation lifespan prediction in the motor was proposed. The model is a combination of FEM and the proposed losses calculation method. To verify the accuracy of the proposed thermal modeling, a test was conducted on the induction motor. The test results and the proposed method results indicated that the temperature rises of the motor increase with the increase of voltage unbalance. The model showed that the impact of the unbalanced voltage on the temperature rise of the motor is more than that of harmonic voltage. As an example, 10% voltage unbalance leads to the temperature rise, and the rotor losses go up about 4%. Moreover, the hotspot of the motor is somewhere between the rotor conductor and close to the stator. This is due to the high flux density and as a result high core losses at that point. Also, compared to other harmonic components the 5th harmonic generates the maximum temperature at different sections of the motor.

9. REFERENCES

1. Agamloh, E. B., ″Induction motor efficiency″, ***IEEE Industry Applications Magazine,*** Vol. 17, No. 6 (2011), 20-28, doi:10.1109/MIAS.2011.942298
2. Al-Badri, M., Pillay, P., and Angers, P., ″A novel algorithm for estimating refurbished three-phase induction motors efficiency using only no-load tests″, ***IEEE Transactions on Energy Conversion***, Vol. 30, No. 2, (2015), 615-625. doi: 10.1109/TEC.2014.2361258
3. Pfingsten, G.V, Steentjes, S. , and Hameyer K., ″Operating point resolved loss calculation approach in saturated induction

machines", ***IEEE Transactions on Industrial Electronics,*** Vol. 31, No. 4, (2016), 1200-1208. doi: 10.1109/TIE.2016.2597761

4. Cabezas Rebolledo, A. A, and Valenzuela M. A., "Expected savings using loss-minimizing flux on induction machine drives—Part I: Optimum flux and power savings for minimum losses", ***IEEE Transactions Industrial Applications,*** Vol. 51, No 2, (2015), 1408-1416. doi: 10.1109/TIA.2014. 2356643
5. Lim, S., and Nam, K., "Loss-minimising control scheme for induction motors", ***IEE Proceedings-Electric Power Applications,*** Vol. 151, No. 4, (2014), 385-397, doi: 10.1049/ ip-epa:20040384
6. Odhano, S. A., Bojoi, R., and Boglietti, A., Rosou, S. G., and Griva, G., "Maximum efficiency per torque direct flux vector control of induction motor drives", ***IEEE Transactions on Industrial Applications,*** Vol. 51, No. 6, (2015), 4415-4424. doi: 10.1109/TIA.2015.2448682
7. Gmyrek, Z., Boglietti, A., and Cavagnino, A., "Estimation of iron losses in induction motors: Calculation method, results, and analysis", ***IEEE Transactions on Industrial Electronics,*** Vol. 57, No. 1, 161-171, (2010) doi: 10.1109/TIE.2009.2024095
8. Kowal, D., Sergeant, P., Dupre, L., and Karmaker, H., "Comparison of frequency and time-domain iron and magnet loss modelling including PWM harmonics in a PMSG for a wind energy applications", ***IEEE Transactions on Energy Conversion***, Vol. 30, No. 2, (2015) 4,76-486. doi: 10.1109/TEC.2014.2373312
9. Reinert, J., Brockmeyer, A., and De Doncker, R. W. A. A., "Calculation of losses in ferro- and ferri-magnetic materials based on the modified Steinmetz equation", ***IEEE Transactions on Industrial Applications.*** Vol. 3, No. 4, (2001), 1055-1061. doi: 10.1109/TEC.2014. 2373312
10. Bradley, K., Cao, W., Clare, J. and Wheeler, P., "Predicting inverter-induced harmonic loss by improved harmonic injection", ***IEEE Transactions on Power Electron***ics, Vol. 23, No. 5, (2008), 2619-2624. doi: 10.1109/TPEL.2008. 2002329
11. Gyselinck, J.J., Dupre, L.R., Vandevelde, L. and Melkebeek, J.A. "Calculation of no-load induction motor core losses using the rate-dependent Preisach model", ***IEEE Transactions on Magnetics,*** Vol. 34, No. 6, (1998), 3876-3881. doi: 10.1109/20.728297
12. Fasil, M., Mijatovic, N., Jensen B. B., and Holboll, J., "Nonlinear dynamic model of PMBLDC motor considering core losses", ***IEEE Transactions on Industrial Electroni***s, Vol. 64 No. 12, ,(2017), 9282-9290. doi: 10. 1109/TIE.2017. 2711536
13. Ruuskanen, V., Nerg, J., Rilla, M., and Pyrhönen, J., "Iron loss analysis of the permanent-magnet synchronous machine based on finite-element analysis over the electrical vehicle drive cycle", ***IEEE Transactions* on *Industrial Electron***ics, 2016, Vol. 63, No. 7, (2016), 4129-4136.doi: 10.1109/TIE. 2016. 2549005
14. Boglietti, A., Cavagnino, A., Ionel, D.M., Popescu, M., Staton, D.A. and Vaschetto, S., "A general model to predict the iron losses in PWM inverter-fed induction motors", ***IEEE Transactions on Industrial Applications*.,** Vol. 46, No. 5, (2010), 1882-1890. doi: 10. 1109/TIA. 2010. 2057393
15. Ionel, D.M., Popescu, M., McGilp, M.I., Miller, T.J.E., Dellinger, S.J. and Heideman, R.J.,"Computation of core losses in electrical machines using improved models for laminated steel", ***IEEE Transactions on Industry Appl*ications**, Vol. 43, No. **7,** (2007), 54-64.doi:
16. Chatterjee, D., "Impact of core losses on parameter identification of three phase induction machines", **IET *Power Electronics,*** Vol. **7**, No 12, (2014), 3126-3136.doi: 10.1049/iet-pel.2014.0121
17. Dlala, E.: "Comparison of models for estimating magnetic core losses in electrical machines using the finite-element method", ***IEEE Transactions on Magnetic*s,** Vol. 45, No. 2, (2014), 716-725.doi: 10.1109/TMAG.2008.2009878
18. A Krings, and J Soulard, "Overview and comparison of core loses models for electrical machines", ***Electrical Energy Conversion***, Vol. 10**,** No 3**,** (2010), 162-169.
19. Dongdong, Z., Ruichi A. and Wu, Z., "Effect of voltage unbalance and distortion on the loss characteristics of three-phase cage induction motor", ***IET Electric Power Applications***, Vol. 12, No. 2, (2018) 264-270. doi: 10.1049/iet-epa.2017.0464
20. Zhao, H., Wang, Y., Dongdong, Z., Zhan, and Luo, Y., "Piecewise variable parameter model for precise analysis of core losses in induction motors", ***IET Electric Power Applications***, Vol. 11, (2017), 361-368, doi: 10.1049/iet-epa.2016.0009
21. Alatawneh N., and Pillay, P., "The minor hysteresis loop under rotating magnetic fields in machine laminations", ***IEEE Transactions on Industrial Applications***, Vol. 50**,** No. 4, (2014), 2544-2553, doi: 10.1109/TIA.2014. 2300155
22. Venkatachalam, K., Sullivan, C.R., Abdallah, T. and Tacca, H., "Accurate prediction of ferrite core loss with non-sinusoidal waveforms using only Steinmetz parameters", 8th IEEE Workshop on Computers in Power Electronics (COMPEL), (2002).
23. Jankowski, T.A., Prenger, F.C., Hill, D.D., O'bryan, S.R., Sheth, K.K., Brookbank, E.B., Hunt, D.F. and Orrego, Y.A.,"Development and validation of a thermal model for electric induction motors", ***IEEE Transactions on Industrial Electronic*s**, Vol. 56, No. 12, (2010), 4043-4054. doi: 10.1109/TIE. 2010. 2043044
24. Boglietti, A., Cossale M., Vaschetto,S., and Dutra, T., "Winding thermal model for short-time transient: Experimental validation in operative condition"s, ***IEEE Transactions on Industrial Applications***, Vol. 5**4,** No**.** 2, (2012), 1312-1319. doi: 10.1109/TIA.2017.2777920
25. Boglietti, A., Carpaneto, E., Cossale, M., and Vaschetto S., "Stator winding thermal models for short-time thermal transients: Definition and validation", ***IEEE on Transactions Industrial Electronic***s, Vol. 63, No. 2**,** (2016), 2713-2721.doi: 10. 1109/TIE.2015.2511170
26. Jankowski, T.A., Prenger, F.C., Hill, D.D., O'bryan, S.R., Sheth, K.K., Brookbank, E.B., Hunt, D.F. and Orrego, Y.A.,"Development and validation of a thermal model for electric induction motors", ***IEEE Transactions on Industrial Electronic***s, Vol. 57, No. 12, (2010), 4043-4054. doi: 10.1109/TIE.2010. 2043044
27. Armando, E. G., Boglietti, A., Castagnini, E. C. A., and Seita, M., "Thermal Performances of Induction Motors for Applications in Washdown Environment", ***IEEE Transactions on Industrial Applications,*** Vol. 55, No. 3, (2019),4578-4585. doi: 10. 1109/ICEL, MACH.2018.8507019
28. Fernando J. T. E. Ferreira, Benoit L., and Aníbal T. De., "Comparison of protection requirements in IE2-, IE3- and IE4-Class motors", ***IEEE Transactions on Industrial Applications***, Vol. 52, No.4, (2016), 3603-3610.doi: 10. 1109/TIA.2016.2545647
29. Ahmed, F. and Kar, N. C., "Analysis of end-winding thermal effects in a totally enclosed fan cooled induction motor with die cast copper rotor", ***IEEE Transactions on Industrial Applications***, Vol. 53, No. 2**,** (2017), 3098-3109. doi: 10.1109/TIA.2017.2648780
30. Boglietti, A., Cavagnino, A., and Popescu, M., and Staton, D., "Thermal model and analysis of wound-rotor induction machine", ***IEEE Transactions on Industrial Application*s**, Vol. 49. No. 5, (2013). doi: 10.1109/TIA. 2013.2261444
31. Zhang, H., "Online thermal monitoring models for induction machines", ***IEEE Transactions on Energy Conversion***, Vol. 30 No. 4, (2015), 1279-1287. doi: 10. 1109/TEC. 2015.2431444

32. Reinert, J., Brockmeyer, A., and De Doncker R. W. A. A., ″Calculation of losses in ferro- and ferri-magnetic materials based on the modified Steinmetz equation″, ***IEEE Transactions on Industrial. Applications***, Vol. 37, No. 4, (2001), 1055-1061. di: 10.1109/28.936396
33. Pry R. H., and Bean, C. P., ″Calculation of the energy loss in magnetic sheet materials using a domain model″, ***Journal of Applied Physics***, Vol. 29, No. 3, (1938), 532-533. https://doi.org/10. 1063/1.1723212
34. Amar A., and Protat, F., ″A simple method for the estimation of power losses in silicon iron sheets under alternating pulse voltage excitation″, ***IEEE Transactions Magnetics***, Vol. 32, No. 2, (1994), 942-944. doi: 10.1109/ 20.312453
35. Emanuel L. B., "Estimation of lifespan expectancies of motors", ***IEEE Electrical Insulation Magazine***, Vol. 8, No. 3, (1992), 5-13. doi: 10. 1109/TDEI. 2002.1024441
36. Pillay, P., and Mthombeni, L. T., "Core losses in motor laminations exposed to high frequency or non-sinusoidal excitation", ***IEEE Transactions Industrial Applications***, Vol. 40, No. 2, (2014), 1325-1332. doi: 10. 1109/TIA.2004.834099
37. Ghorbanian, V., Faiz, J., Sabouri, M., and Ojaghi, M., ″Exact modeling and simulation of saturated induction motors with broken rotor bars fault using winding function approach", ***International Journal of Engineering, Transactions A: Basics***, Vol. 27, No. 1, 69-78. doi: 10.5829/idosi.ije.2014.27.01a.10
38. Yektaniroum, T., Niaz Azari, M., and Gholami, M., "Optimal rotor fault detection in induction motor using particle-swarm optimization optimized neural network." ***International Journal of Engineering, Transactions B: Applications***, 2018, Vol. 31, No. 11, 1876-1882. doi: 10.5829/ije.2018.31.11b.11

Persian Abstract

چکیده

موتورهای الکتریکی القایی در طیف گسترده ای از شرایط و موارد صنعتی مورد بهره برداری قرار می گیرند. امروزه موتورهای جدیدبا استفاده از مواد جدید و روش های بهبود یافته و برای محدوده های مختلف توان طراحی شده اند، وگرچه اغلب بسیار کوچکترندولی بارگذاری بیشتری دارند. برای حصول اطمینان از طول عمر رضایت بخش موتورها ، افزایش دما باید به مقادیر ایمن محدود شود. در این مقاله با لحاظ کردن هارمونیک های منبع تغذیه یا عدم تعادل ولتاژ آن, یک رویکرد تحلیلی برای تخمین تلفات اصلی موتورهای القایی ارائه شده است. با معرفی یک مدل حرارتی مبتنی بر پارامترهای فشرده حرارتی, طول عمر عایق موتورهای القایی پیش بینی شده است. شبکه پارامترها بر اساس ابعاد موتورها، مقاومت های حرارتی، خازن های حرارتی و منابع اتلاف بنا شده است. سپس، این مدل برای تخمین دمای قسمت های مختلف موتور ونبز تعیین طول عمر عایق آن به کاررفته است. سرانجام ، نتایج پیش بینی شده از مدل توسط آزمایش های لازم مورد تأیید قرارگرفته است.